The sub-µm petrography of the observed meteorite fall Winchcombe—A complex array of pristine and altered chondrite components

Johannes LIER[1], Christian VOLLMER [ID][1]*, Linus RISTHAUS[1], Demie KEPAPTSOGLOU[2,3],
Quentin M. RAMASSE[2,4], Aleksander B. MOSBERG[2], Ashley J. KING [ID][5], Charlotte L. BAYS[5,6], and
Paul F. SCHOFIELD[5]

[1]Institut für Mineralogie, Universität Münster, Münster, Germany
[2]SuperSTEM Laboratory, Daresbury, UK
[3]School of Physics, Engineering and Technology, University of York, Heslington, UK
[4]School of Chemical and Process Engineering and School of Physics and Astronomy, University of Leeds, Leeds, UK
[5]Planetary Materials Group, Natural History Museum, London, UK
[6]Department of Earth Sciences, Royal Holloway, University of London, Egham, UK

*Correspondence
Christian Vollmer, Institut für Mineralogie, Universität Münster, Corrensstr. 24, 48149 Münster, Germany.
Email: cvoll_01@uni-muenster.de

Abstract–Samples of observed meteorite falls provide important constraints on alteration histories of Solar System materials. Due to its rapid collection, terrestrial alteration in the observed Mighei-type (CM) carbonaceous chondrite fall Winchcombe was minimal. In this work, the petrography and mineralogy of three Winchcombe lamellae, two from the matrix and one from a lithological clast, were analyzed by transmission electron microscopy. Our results demonstrate that the matrix of Winchcombe is dominated by Mg-Fe-rich serpentine-type phyllosilicates and tochilinite-cronstedtite intergrowth (TCI)-like phases with variable, but generally high (petrologic type 2.0–2.3) alteration degrees that agree with petrologic types acquired on TCIs on larger scales in other work. However, we also located pristine areas in investigated lamellae such as homogeneous amorphous silicates and glassy particles with sulfide and metal inclusions that resemble altered cometary GEMS (glass with embedded metal and sulfides). One distinct GEMS-like domain shows Fe-rich metal and sulfide grains with oxygen-enriched rims in a Mg-rich amorphous groundmass embedded in organic matter, which likely shielded it from more severe alteration. Fe-Ni-sulfides are mainly pentlandite and concentrated in matrix lamellae. In addition to the sub-µm scale brecciated texture, the three lamellae show different alteration extents, further demonstrating the complex alteration nature of this CM2 meteorite.

INTRODUCTION

The study of Mighei-type (CM) carbonaceous chondrites and their alteration history is crucial to understanding the formation and evolution of our solar system (e.g., Suttle et al., 2021). However, the timing and location of aqueous alteration on the CM parent body are complex. These alteration processes were facilitated by fluids from melted water–ice grains in the accretionary assemblage (e.g., Brearley, 2006; Suttle et al., 2021; Tomeoka & Buseck, 1985). The presence of centimeter-scale alteration fronts at the thin section scale is evidence for parent body-hosted alteration, as well as mineralized veins, which cut through both matrix and chondrules, large phyllosilicate clusters, and the redistribution of soluble elements from refractory inclusions into the matrix (Lee et al., 2012). On the other hand, Metzler et al. (1992) presented petrographic

observations which imply that hydrous silicates partly formed prior to the accretion of the CM parent body. They concluded that evidence for both pre-accretionary and post-accretionary hydration processes is found in CM chondrites. Evidence from modeling shows that chondrule-forming shock waves in icy regions of the nebula produced conditions that allowed rapid mineral hydration (Ciesla et al., 2003). This class of meteorites therefore records varying degrees of aqueous alteration covering a wide petrologic range from mild to fully hydrated (King et al., 2022).

It is hypothesized that initial amorphous silicates, metal, and sulfides in the matrix were converted into Fe-bearing serpentines (cronstedtite) and hydrous sulfides (tochilinite) followed by serpentinization of refractory coarse-grained silicates, which led to the addition of Mg to the fluid (Leroux et al., 2015; Rubin et al., 2007; Tomeoka & Buseck, 1985). Phyllosilicates are therefore the most abundant alteration products found in CM chondrites, followed by TCIs and other common alteration minerals such as carbonates and iron oxides (e.g., Barber, 1981; Hewins et al., 2014; Pignatelli et al., 2016; Zega et al., 2006; Zolensky et al., 1993). A recent study by Marrocchi et al. (2023) stated that amorphous silicates were hydrated before accretion of the CM parent body, which could indicate an even more complex alteration scenario.

Of particular interest are TCIs that are usually not found in other chondrite groups, and whose formation mechanisms and precursors are still not fully understood (e.g., Fuchs et al., 1973; Mackinnon & Zolensky, 1984; Nakamura & Nakamuta, 1996; Pignatelli et al., 2016, 2017). Cronstedtite forms a solid solution with greenalite and chrysotile, the products of which occur in CM2 chondrites (Velbel, 2014). TCIs may also contain minor amounts of magnetite, chromite, and minerals containing Fe, Ni, Cr, and P like schreibersite. Based on their petrographic context, texture, and composition, TCIs are further divided into type-I and type-II TCIs. Type-I TCIs are thick, rounded, sulfur-rich, and mainly composed of tochilinite with variable amounts of cronstedtite and magnetite (Nakamura & Nakamuta, 1996). Tomeoka and Buseck (1985) proposed that type-I TCIs formed by low-temperature interaction of S-bearing fluids with kamacite. As the alteration degree and fragmentation of chondrules increased, more cronstedtite was produced instead of tochilinite. Type-II TCIs consist of tochilinite, cronstedtite, and Fe-hydroxides, show fibrous textures, have a complex chemical zoning, and occur exclusively in the matrix as fibrous clumps originated from the pseudomorphism of anhydrous silicates (Pignatelli et al., 2016, 2017). TCIs with intermediate amounts of cronstedtite have not been observed yet, which suggests the existence of distinct precursors to explain the occurrence of two distinct types of TCIs (Pignatelli et al., 2016, 2017). Mellilite, troilite, and Ca-carbonates have been proposed as possible precursors for type-II TCIs (Lee et al., 2013). Hydrothermal experiments by Vacher et al. (2019) have shown that tochilinite likely formed from the alteration of Fe-Ni metal beads in an S-bearing alkaline environment at low temperature (i.e., <160°C). Tochilinite and cronstedtite both crystallized at 80°C in the experiments, leading them to conclude that these minerals formed at the same temperature during aqueous alteration in CM chondrites. Another recent study of the Winchcombe meteorite by Daly et al. (2024) pointed out that phase heritage from TCI-like objects would suggest that carbonates may have been a greater component of CMs during early aqueous alteration than currently thought.

Different degrees of aqueous alteration in CM chondrites can be classified by various mineralogical, petrological, and textural parameters. Rubin et al. (2007) and Rubin (2015) assigned petrologic subtypes ranging from 2.7 to 2.0 (highly altered samples), with this scale extended by Kimura et al. (2020) to 3.0–2.8. Lentfort et al. (2021) proposed that the subclassification can be approximated by considering only the "FeO"/SiO_2 ratio of TCIs. They studied 27 thin sections of 19 different CM chondrites and defined new subtypes (CM2.7–CM2.9) to allow a precise classification of samples and lithological units with low degrees of aqueous alteration. However, these alteration schemes need to be tested and applied on new types of meteorites and specifically meteorite falls, where the effects of terrestrial alteration can be largely excluded.

The Winchcombe meteorite is one of the least terrestrially altered CM chondrites as its main mass was collected only ~12 h after its fall in February 2021, with a total of 531.5 g of material recovered less than 7 days after the fall. Precise documentation of the meteorite fall allowed the calculation of its pre-atmospheric orbit and confirmed the link between CM chondrites and hydrated main belt C-type asteroids thought to originate in the outer solar system (King et al., 2022). The pristine nature of the sample combined with its precise outer main asteroid belt origin makes this meteorite the ideal candidate for investigating the geological history of the CM chondrite group (Suttle et al., 2024). Initial observations of polished samples (King et al., 2022) showed that Winchcombe is a heterogeneous breccia with multiple distinct lithologies. More extensive studies by Suttle et al. (2024) on 16 polished sections identified eight distinct lithologies (A–H), all classified as CM chondrite clasts. The different lithologies represent a range of alteration extents with variable matrix textures from advanced aqueous alteration (CM2.0–2.3) to mildly altered (CM2.6). They confirmed that generations of

different alteration, disruption, and re-accretion might have occurred on the CM parent body.

Roughly 85% of the studied area was assigned by Suttle et al. (2024) to a specific lithology, whereas the remaining ~15% comprised a mix of materials with no coherent alteration extent assigned as "matrix". This matrix was previously described as fragmented and "cataclastic" (Suttle et al., 2024). This fine-grained (<10 µm) material occurs as small regions adhering to the edges of lithological clasts, which generally have a coarser-grained (>10 µm) texture. The matrix consists of subangular fragments of typical CM chondrite components such as sulfides, chondrules and chondrule fragments, olivine and pyroxene, carbonates, TCI clusters, and fine-grained phyllosilicates. The matrix is therefore a complex mix of components with both heavily altered and mildly altered phases in close association. The descriptive term "cataclastic" used by Suttle et al. (2024) should be regarded with caution, as it usually describes a rock produced by dynamic metamorphism in discrete zones of differential stress and movement, for example, fault-thrust zones and shear zones. This definition by Wise et al. (1984) emphasizes the fact that recrystallization through high stress takes place (metamorphism), which is not the case for the matrix in Winchcombe. Additionally, Metzler et al. (1992) also investigated CM chondrite matrix in detail and did not use the term "cataclastic," but "clastic." We will therefore stick to the older definition and use the term "clastic" throughout the paper.

The nature of the fine-grained Winchcombe matrix, chemical compositions of minerals, and their textural relationships on a sub-µm scale have not been investigated in detail yet. These investigations are important to understand the nature of complex alteration trends on the CM parent body. In this study, three electron-transparent lamellae from Winchcombe were studied by transmission electron microscopy (TEM) techniques to evaluate high-resolution phyllosilicate crystallography and TCI chemical compositions. The mineralogy and chemical compositions of accessory phases were also analyzed including amorphous areas that resemble GEMS-like particles ("glass with embedded metal and sulfides") (Leroux et al., 2015). Furthermore, the functional chemistry of organic matter associated with the "GEMS-like" material was investigated by synchrotron-radiation Scanning Transmission X-ray Microscopy (STXM).

METHODS

Electron-transparent lamellae were prepared from polished section P30544 (BM.2022, M2-46) of the Winchcombe meteorite (size ~2.5 mm^2), curated by
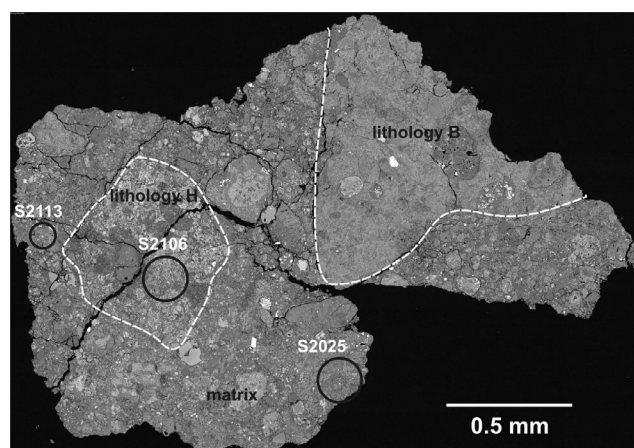

FIGURE 1. SEM micrograph of the Winchcombe section P30544 (BM.2022, M2-46), from which the FIB lamellae have been extracted. The lamellae originate from lithology H in Winchcombe (S2106) as well as the clastic matrix (S2025 and S2113).

the Natural History Museum (NHM), London, UK (Figure 1). A large fraction of the thin section (~1.4 mm^2) is composed of the clastic matrix described above. We extracted two random lamellae from this matrix region ("S2025" and "S2113") and one lamella from the more altered lithology H ("S2106"), which is the least abundant lithology of Winchcombe and where a petrologic sub-type of 2.3/2.4 was assigned (Suttle et al., 2024). All lamellae were prepared on a Hitachi Ethos NX5000 Focused Ion Beam-Scanning Electron Microscope (FIB-SEM) (3 kV) at the SuperSTEM laboratory, Daresbury, UK using standard FIB preparation protocols.

Lamellae were investigated with the aberration-corrected (objective system) ThermoFisher Scientific "Themis" TEM at the University of Münster. This TEM works at an acceleration voltage of 300 kV and is equipped with a high-brightness field emission gun (X-FEG), a Wien-filter type monochromator, a four-quadrant silicon-drift energy-dispersive X-ray (EDX) detector (SuperX technology), a Fischione Model 6000 high-angle annular darkfield (HAADF) detector, and a fast CMOS camera (Ceta 4 k × 4 k). We performed conventional brightfield (BF), high-resolution (HR) imaging (usually down to 0.1 nm with the corrected objective system), and selected area electron diffraction (SAED) to document the texture and crystallography of the lamellae. HR images were analyzed using the Gatan Microscopy Suite, and crystallographic interplanar spacings ("d-values") were compared to the American Mineralogist Crystal Structure Database (Downs & Hall-Wallace, 2003). Spectrum images, where complete EDX spectra are acquired on every pixel, were acquired in scanning TEM (STEM) mode (condensor aperture 50 µm, beam convergence 15.7 mrad) using beam
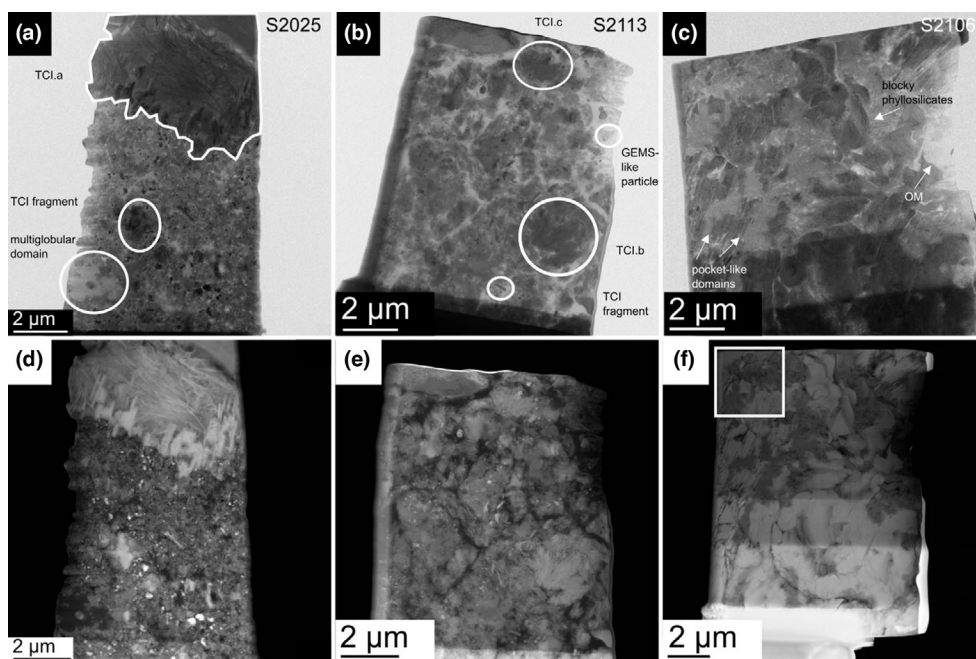
FIGURE 2. TEM overview micrographs of the three lamellae S2025 (a, d), S2113 (b, e), and S2106 (c, f) in TEM-BF (top row) and STEM-HAADF (bottom row). The arrow in (c) marks an organic domain that was also analyzed in Vollmer et al. (2024). The rectangle in f) reveals the section that contains a calcite grain (Figure S1f).

currents of about 500–800 pA and analysis times of 100–200 µs px^{-1}, with several hundred frames summed up to achieve sufficient counting statistics. We quantified STEM-EDX data using the Velox software (ThermoFisher Scientific).

One carbonaceous region in lamella S2113 was additionally investigated by STXM and X-ray absorption near-edge structure (XANES) at the I08 beamline of Diamond Light Source (DLS), UK. Spatially correlated energy dependent image stacks (~5 × 3 µm, 100 × 60 pixels) were acquired at the carbon (278–310 eV) K-edge with a nominal beam size of ~40 nm and a dwell time per pixel of 10 ms, with a step size of 0.1 eV over the main edge and between 0.2 and 0.5 eV across the rest of the scan.

RESULTS

General Petrography

The overall petrography of the three samples demonstrates the heterogeneous character of the Winchcombe matrix on the sub-µm scale, with all three lamellae characterized by subtle mineralogical differences (Figure 2). Lamella S2025 consists of a fine-grained (<1 µm) assemblage of different phases intermixed with organic matter and a platy to fibrous micron-sized TCI-like (TCI.a) grain with strong diffraction contrast on one side. Lamella S2106, on the other hand, shows a smoother, intergrown texture with larger (>1 µm) phases partly protruded by acicular or blocky grains. Finally, S2113 consists of nano- to micron-scale grains ranging from rounded to scaly-fibrous permeated by vein-like carbon-rich material. Generally, all three lamellae are characterized by abundant carbonaceous material intermixed with the matrix (Figure S6). Rarely, this organic matter occurs as larger grains; for example, in one corner of lamella S2025 with a large (~ 2 µm) cluster of multiglobular organics (Figure 2a,d). The functional chemistry and textures of these organic grains are the topic of a separate paper (Vollmer et al., 2024), in which, for example, an organic domain from S2106 was analyzed (Figure 2c; S2106 = FIBW07 in their paper).

In lamella S2113, we also found an apatite grain with well-developed crystal faces (Figure S1a), an almost 500 nm long domain containing significant amounts of only Al and O, which is likely a corundum grain (Figures S1b,c and S9), and an Fe,Ni,P-phase within a TCI grain (Figure S1d). We also observed some Ca-carbonates, for example, in lamella S2106 with a µm-sized calcite on the edge of the lamella (Figure S1f). Generally, we did not characterize accessory minerals such as carbonates or apatites in further detail and instead focused on major phases in the analyzed lamellae, which we will discuss below.
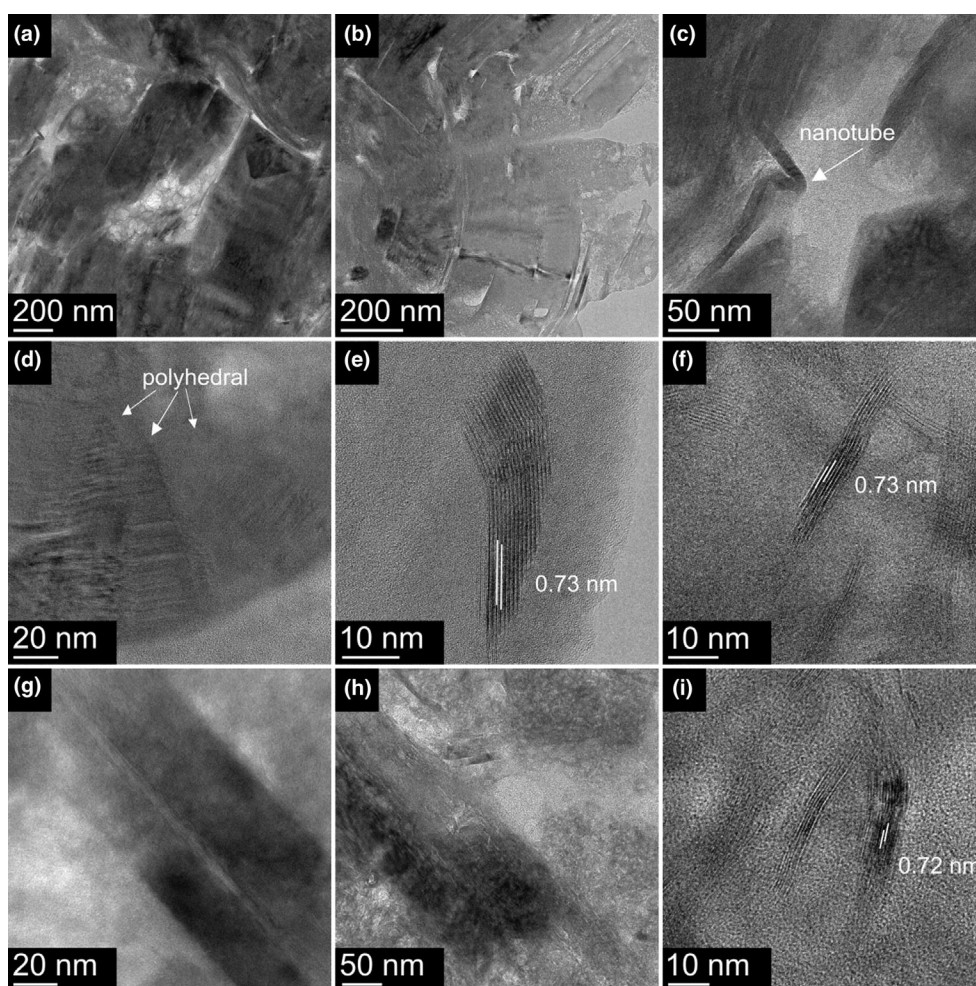
FIGURE 3. TEM micrographs and HR images of typical phyllosilicate textures in Winchcombe. In lamella S2106, blocky and polyhedral textures dominate (BFTEM: a, b), and a distinct nanotube points to the chrysotile polymorph (HRTEM: c). In S2113, polyhedral lizardite (BFTEM: d) and Mg-serpentine fibers occur frequently (HRTEM: e, f). In S2025, blocky Fe-rich serpentines, likely cronstedtite, occur (BFTEM: g, h), but tiny serpentine fibers are also present (HRTEM: i).

Phyllosilicates

Phyllosilicates occur in all three lamellae with different textures varying from fibrous to blocky, lath-shaped, and rounded (Figure 3). They are mostly below 1 μm in size. The most common textures are fibrous phyllosilicates ranging from a few nm to several μm in length, which are often only a few nanometers thick (Figure 3e,f,i). In addition to the fibrous texture, blocky and lath-shaped crystals also occur, dominantly in lamella S2106 (Figure 3a,b, Figures S3a and S7c–e). In this lamella, packages of rounded and blocky phyllosilicates make up almost 80% of the observed surface area.

In HRTEM mode, we could analyze the nanoscale crystallography of phyllosilicates. The most common d-value is ~0.72–0.73 nm (Figure 3e,f,i), which fits to a known main d-spacing in chrysotile that is abundant in S2025 and S2113. Some curved nanotube-like fibers are also observed (Figure 3c), which are typical for this polymorph of serpentine-type minerals. Other phyllosilicates such as clay minerals (e.g., smectites) characterized by d-values >1 nm (excluding tochilinite discussed below) were not found. In one fibrous assemblage in S2025, d-values could not be accurately determined, and the range of d-values from 0.7 to 1 nm could either indicate a serpentine mineral, the (001) plane of tochilinite, or a clay mineral like saponite (Figure S2a,b). In S2113, a platy and polyhedral domain shows two distinct d-values of 0.72–0.73 and 0.45 nm, which match well to lizardite (Figure 3d, Figure S5). This domain shows an increased Mg content by EDX, which could be due to an alteration front (Figure S5a,b).
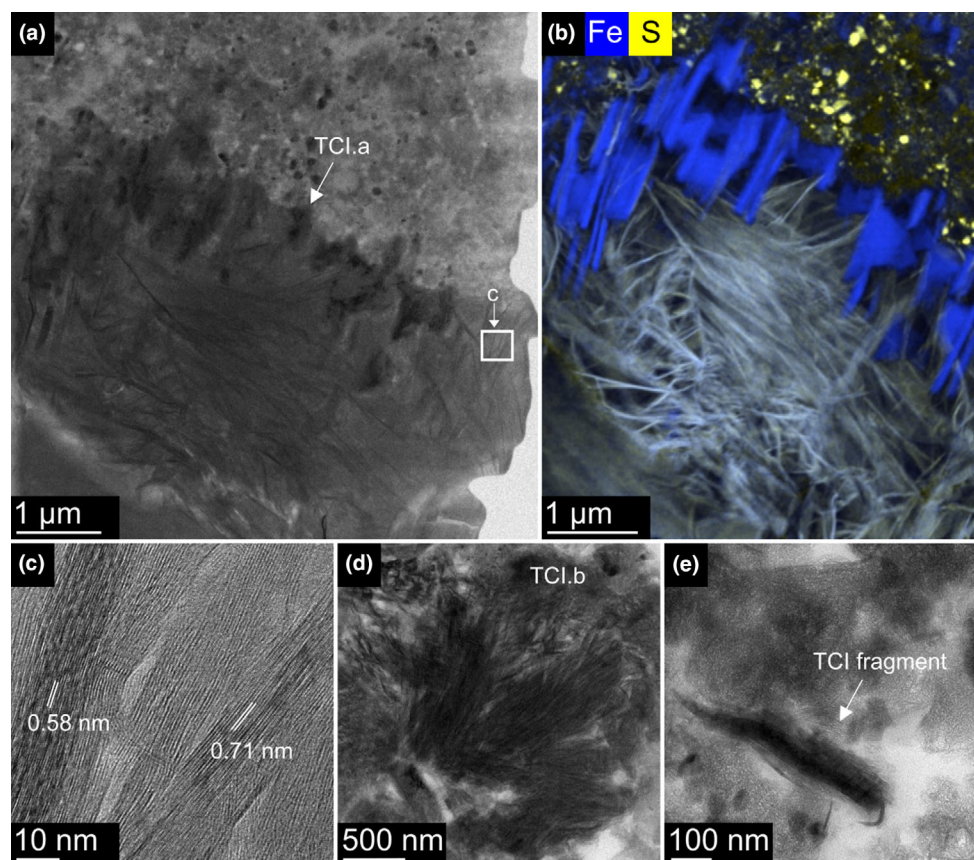
FIGURE 4. TEM micrographs and a STEM-EDX map of typical TCI textures in Winchcombe. (a) S2025 contains a large TCI grain (TCI.a) with blocky and fibrous compounds (BFTEM). (b) The outer edge of the TCI is dominated by blocky cronstedtite with a preferred orientation (STEM-EDX mapping with Fe-blue and S-yellow, overlaid on top of the HAADF image). (c) The HRTEM image of one TCI.a area ("c" in panel a) confirms the complex intergrown crystallography of this asbestiform material. (d, e) In S2113, radial TCIs as well as blocky, irregular fragments occur (BFTEM).

TCI-Like Phases

TCIs are one of the most characteristic alteration phases in CM2 chondrites, and similar phases are observed in all three lamellae with morphologies comparable to those described previously (Pignatelli et al., 2016; Suttle et al., 2024). However, in our sample set, fibrous and radial domains similar to type II TCIs are more common than blocky type I TCIs (Figure 4). In lamella S2025, a ~6.5 μm large TCI-like grain dominates the outer portion of the lamella, in which fibrous tochilinite in the center and blocky Fe-rich phyllosilicates in the rim intercalate, showing a diagonal preferred orientation (Figure 4b).

This phase ("TCI.a", Figure 2a) covers an area of ~21 μm^2 and is therefore the largest TCI-like grain in all three lamellae. In its center, it has a fibrous texture with needle-like tochilinite intergrown with more Mg-rich serpentine-type phases. Toward the rim, platy Fe-rich phyllosilicate crystals with a layered texture occur. We

investigated the chemistry of TCI.a with two measurements, one ignoring (TCI.a) and one including the platy Fe-rich phyllosilicates (TCI.a*) (Table 1, Table S1, Figure S8a–c). The atomic Mg/(Mg + Fe) value of the whole TCI.a* is ~0.43 and without the Fe-rich phyllosilicates ~0.51. We also investigated TCI-like grains in some regions by HR imaging and could document d-values of both cronstedtite and the hydroxysulfide portion of about 0.71 and 0.58 nm (Figure 4c), respectively, which indicates a slight deviation from the value of tochilinite reported in the literature (~0.54 nm) (Mackinnon & Zolensky, 1984). Further blocky and fibrous fragments that are texturally similar to the large TCI.a grain also occur in other regions of the lamella, for example, in the middle and the opposite side (Figure 2d). The largest of these fragments in the middle of the lamella has a diameter of ~1.5 μm. A similar TCI-like fragment in S2025 is mostly comprised of cronstedtite and shows a similar platy and layered texture (Figure S3b). In S2113, two micron-sized (~1.8

TABLE 1. Compositions of the three major TCI-like phases in Winchcombe FIB sections S2025 and S2113 (1 σ errors). Two analyses were performed on TCI.a, one without (TCI.a) and one with the coarser-grained Fe-rich phyllosilicates (TCI.a*). The target areas of the analyses can be seen in Figure S8.

Fraction	Atom%							
Element	TCI.a	±	TCI.a*	±	TCI.b	±	TCI.c	±
O	61.40	2.26	59.88	2.14	54.48	2.09	51.61	2.84
Na	0.40	0.08	0.21	0.04	0.45	0.09	0.83	0.17
Mg	11.26	2.04	10.13	1.85	7.48	1.41	13.39	2.41
Al	1.18	0.23	1.27	0.25	1.97	0.39	1.54	0.31
Si	11.28	1.96	11.83	2.03	12.23	2.09	14.8	2.53
S	3.36	0.62	2.89	0.53	4.41	0.80	4.43	0.82
K	0.02	0.00	0.02	0.00	0.04	0.01	0.05	0.01
Ca	0.04	0.01	0.05	0.01	0.05	0.01	0.09	0.01
Fe	10.62	1.32	13.33	1.59	18.55	2.08	12.92	1.65
Ni	0.42	0.06	0.38	0.06	0.34	0.05	0.34	0.05

Fraction	wt%							
Element	TCI.a	±	TCI.a*	±	TCI.b	±	TCI.c	±
O	41.94	2.20	39.30	2.08	32.75	1.97	32.81	2.42
Na	0.39	0.08	0.20	0.04	0.39	0.08	0.76	0.16
Mg	11.68	2.13	10.10	1.88	6.83	1.33	12.93	2.36
Al	1.36	0.27	1.40	0.28	2.00	0.41	1.65	0.34
Si	13.53	2.32	13.63	2.35	12.91	2.27	16.52	2.79
S	4.60	0.85	3.80	0.71	5.31	0.99	5.64	1.05
K	0.03	0.01	0.03	0.00	0.07	0.01	0.08	0.02
Ca	0.08	0.01	0.09	0.01	0.07	0.01	0.15	0.02
Fe	25.33	2.70	30.53	3.01	38.92	3.37	28.67	3.05
Ni	1.06	0.16	0.92	0.14	0.75	0.12	0.79	0.12

and ~ 1.3 μm) TCI-like grains (TCI.b, TCI.c) have a circular fan-like shape with a fine-fibrous texture, needle-like crystal growth and preferred orientation (Figure 2b). In contrast to TCI.a in S2025, both TCI.b and TCI.c grains do not show any platy crystal morphologies. In this lamella, a blocky TCI fragment with d-values of 0.57 and 1.1 nm is evident in HR images, pointing to the hydroxysulfide portion of the TCI (Downs & Hall-Wallace, 2003; Mackinnon & Zolensky, 1984) (Figure 4e; Figure S2e,f). Chemical compositions of the three TCI-like grains vary greatly in their O, Mg, Si, and Fe contents (Table 1).

For example, TCI.b is depleted in Mg (6.83 wt%) in comparison with TCI.c (12.93 wt%). The largest disparities are observed in their Fe contents, ranging from 25.33 and 30.53 wt% in TCI.a/a* to 38.92 wt% in TCI.b. TCI.a and TCI.c have a S/SiO_2 ratio of 0.16, TCI.a* has a lower ratio of 0.13, and TCI.b has a higher ratio of 0.19. The "FeO"/SiO_2 ratio for TCI.a without is 1.13, and with the Fe-rich phyllosilicates for TCI.a* is 1.35. TCI.b has the highest ratio at 1.81, while TCI.c has the lowest at 1.04 (Table 1). Additional elemental maps and the ROIs of the TCI-like grain analyses are provided in Figure S8.

No d-values could be measured in S2106 to confirm the presence of tochilinite, but element maps show that some phyllosilicates are enriched in sulfur (Figure S6) indicating the occurrence of TCI grains in this lamella as well. The chemistry of the phyllosilicates of the TCI-like phases is shown in Figure S10 (composition in atom%) revealing the solid solution of cronstedtite, antigorite, and greenalite.

Sulfides

Sulfides are widespread in lamellae S2113 and S2025 with not only rounded or sub-rounded but also euhedral crystal shapes (Figure 5). Pentlandite is the dominant sulfide with variable sizes of <100 nm to several 100 nm and strong diffraction contrast. The sulfides are occasionally surrounded by organic matter or carbon-rich phases that were not characterized any further in this work. Several rounded phases with three distinct d-values of 0.58, 0.50–0.46, and 0.35 nm and sizes of a few tens of nm up to 300 nm in size were identified. These values correspond to the (111), (200) and (220) lattice planes of pentlandite (Downs & Hall-Wallace, 2003). STEM-EDX data confirm the high Ni content of pentlandite grains (Figure S6a,d). Their abundance is higher in S2025 than in S2113, and in some areas, they form distinct clusters (Figure 5d). Some of them show well-developed crystal
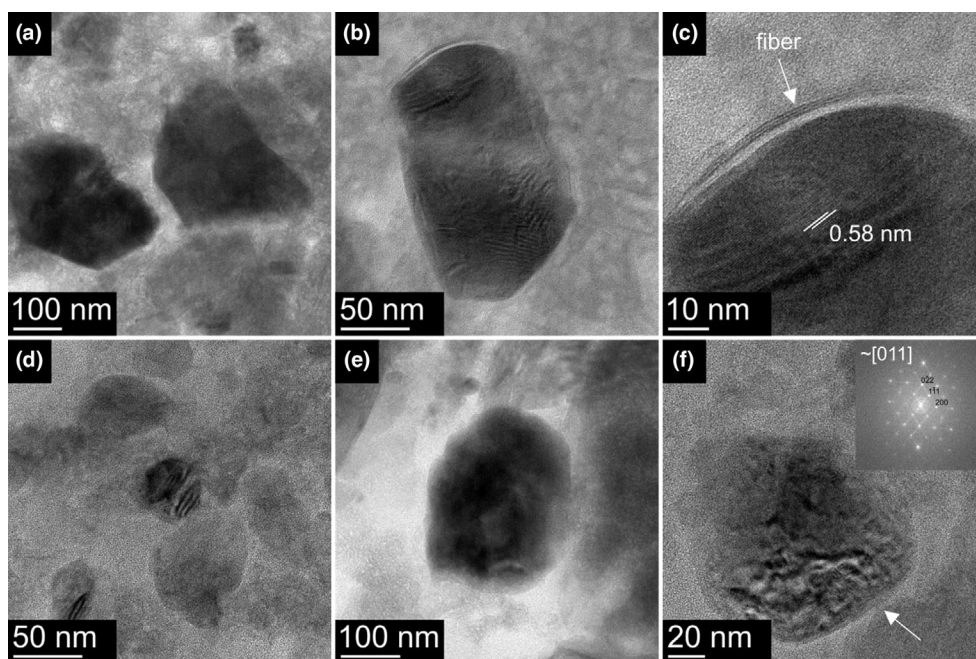
FIGURE 5. TEM micrographs and typical textures of sulfides in Winchcombe. In S2025, the sulfides, mainly pentlandite, not only show euhedral (BFTEM: a), but also rounded morphologies (HRTEM: b, c). In S2113, the sulfides are mainly rounded (BFTEM: d, e). In some regions, HRTEM imaging and FFT analysis could be indexed to a pentlandite zone axis (f). This sulfide as well as other grains seem to be surrounded by an amorphous carbon-rich rim (arrow).

faces (Figure 5a). In some areas, overlapping grains form Moiré fringes (Figure 5d), which indicate distinct platy crystal shapes overlapping each other. In addition, one of the pentlandite grains that shows a strong (111) diffraction signal is surrounded by a small, elongated grain of a few nm in thickness, which is likely a serpentine fiber from a subsequent alteration episode (Figure 5c). However, a precise d-value could not be determined due to its very small size and orientation. Additionally, $Ni/(Fe + Ni)$ values were calculated from element maps (Figure S6a,d), with the pentlandites in S2025 having a $Ni/(Fe + Ni)$ value of 0.5 ± 0.04 and the ones in S2113 0.4 ± 0.04. These values confirm the identification as pentlandite (Chokai et al., 2004). In S2106, the number of sulfides in general and of Fe-Ni-sulfides is much lower than in the other two lamellae, and there seems to be a comparable amount of FeS phases (Figure S6g) indicated by STEM-EDX maps. Unfortunately, d-values could not be analyzed (Figure S6g).

GEMS-Like Phases and Amorphous Silicate Material in S2106 and S2113

In some regions, amorphous silicate domains occur (Figures 6 and 7). Specifically, in lamella S2113, we discovered a distinct ~300 nm-sized grain (Figure 6a,b) with a texture and composition that resembles a "glass with embedded metal and sulfides" (GEMS)-like grain similar to what was described in the CM chondrite Paris (Leroux et al., 2015) (Table 2). The grain is surrounded by organic matter with a sharp boundary. Investigations by STXM indicate a high aromaticity content and the typical carbon K-edge functional chemistry of extraterrestrial organic matter found in meteorites (Figure 8). The diameters of the rounded inclusions vary between ~10 and 60 nm. Most of the included phases show rims of ~4 nm. STEM-EDX data indicate that the rims are slightly enriched in oxygen and have a lower mass number (Figure 6d–f, Figure S4b). The groundmass of the GEMS-like grain is an amorphous silicate that contains Fe, Mg, Al, and Si (Figure S4a,c,d). It is also characterized by very low crystallinity, confirmed by HR imaging and corresponding Fast Fourier Transformation (FFT) patterns (Figure 6g), but in some regions, fibrous minerals, likely serpentines, are observed (Figure 6h). Embedded in the silicate glass are two pentlandite grains with Ni-contents of 32.0 and 27.7 wt%, calculated from the element map that is shown in Figure 6b. One pentlandite shows d-spacing with d-values of 0.57, 0.50, and 0.35 nm (Figure 6c). Additionally, a Ni-poor (~1 wt %) pyrrhotite or troilite with a size of ~50 nm width and 80 nm length and with only one meaningful d-value of 0.52 nm (Figure 6e) was found in the top-right corner of the phase. The GEMS-like phase also contains several
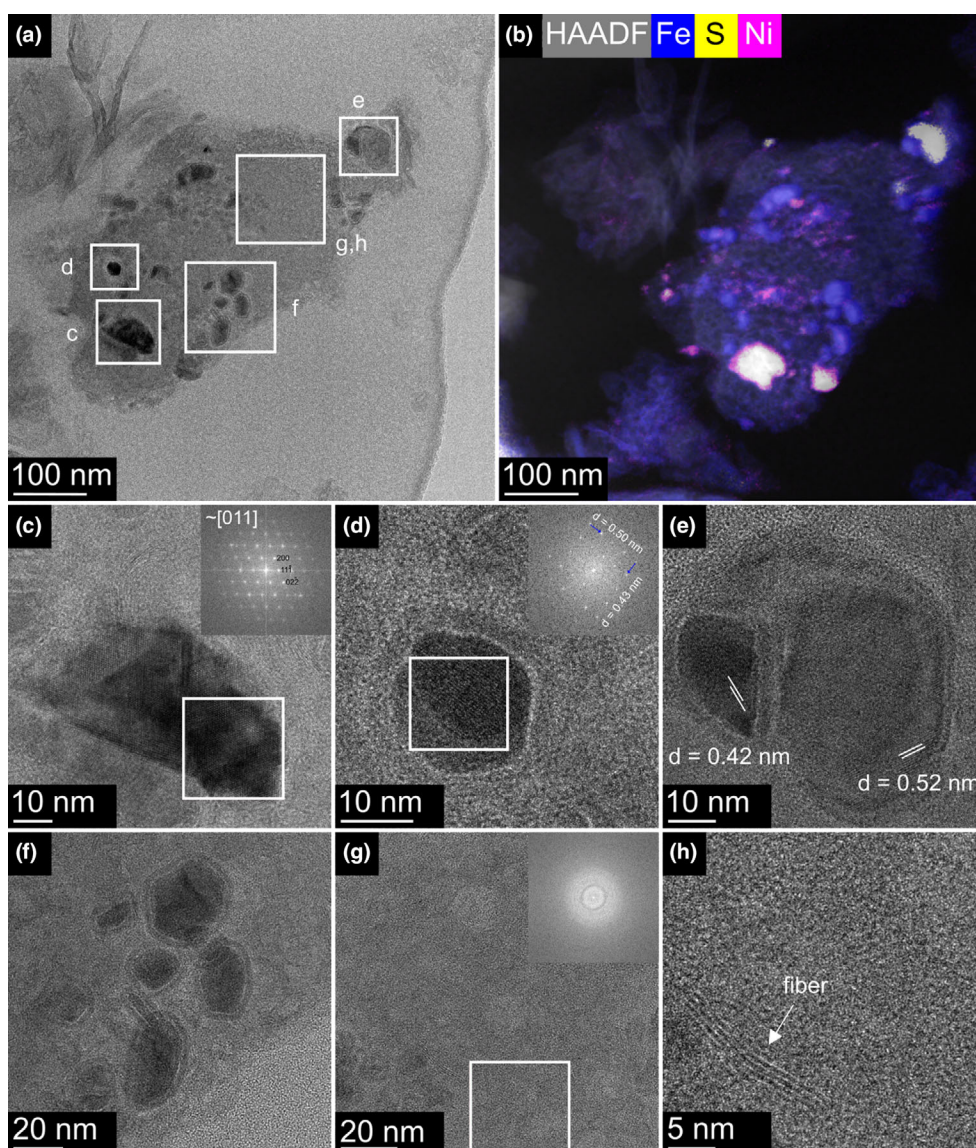
FIGURE 6. TEM micrographs and EDX map of an amorphous GEMS-like phase in S2113. (a) BFTEM image of the GEMS-like phase and the composite HAADF-EDX map (b) show rimmed and un-rimmed Fe-rich inclusions within an amorphous groundmass. HRTEM imaging and FFTs of the Fe-S-rich inclusions could be tentatively indexed to pentlandite (c) and pyrrhotite/troilite with a Fe-rich nano-inclusion to the left (e). The Fe nano-inclusions in (d) and (e, on the left) show larger d-values that do not fit to kamacite. Some Fe-rich, rounded inclusions whose rims are ~3 nm thick occur as clusters and have smaller d-values comparable to kamacite (f). The amorphous state of the groundmass of this domain can be confirmed by the FFT (g). Small proto-phyllosilicate fibers are also found in the groundmass (h).

Fe-rich phases without sulfur, which are exclusively found in this grain. The d-values of one of these particles could match the (111) planes of magnetite with ~0.5 nm (Figure 6d), but are too large for kamacite or wustite.

The second GEMS-like region in S2113 is much smaller and characterized by three internal phases embedded in an amorphous groundmass (Figure 7a,b). One of the three inclusions shows a d-value of ~0.2 nm and cannot be clearly identified. The second inclusion shows a good diffraction contrast, and the measured d-

value of 0.34 nm fits with a slight deviation to the (220) series of pentlandite.

In lamella S2106, pocket-like amorphous silicate phases occur that are embedded in phyllosilicate-dominated packages and contain rounded and rimmed inclusions (Figure 7d–f and Figure S7a,b). No d-values could be determined due to the thickness of the lamella in those regions. However, the composition of one pocket-like domain in S2106 could be determined (Table 2, Figure S7b). The EDX data from this region indicate a
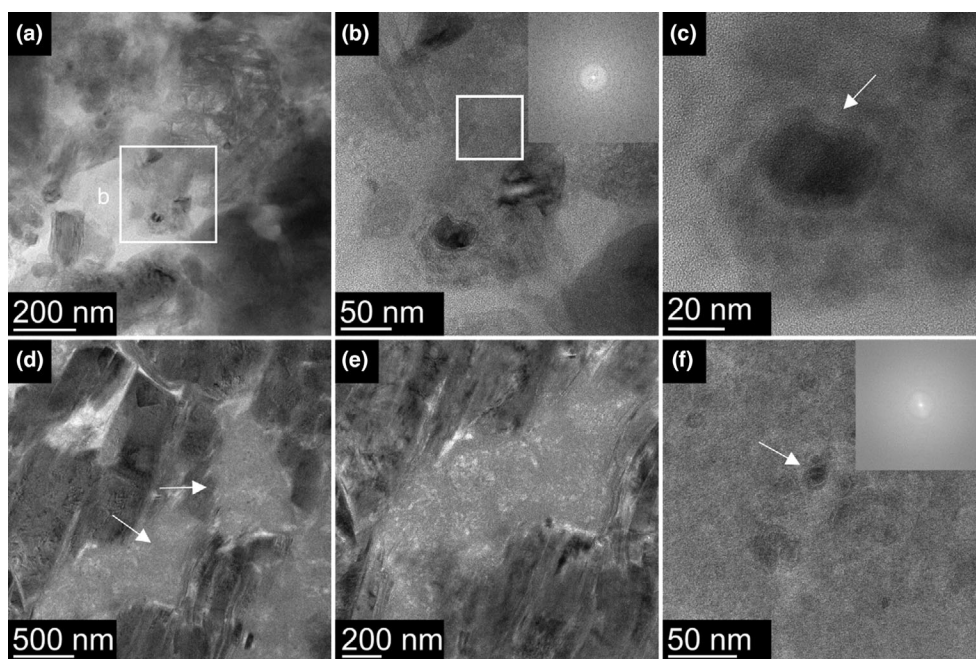
FIGURE 7. TEM micrographs of further amorphous silicate textures in the Winchcombe matrix. In S2113, a second GEMS-like phase was found (BFTEM: a). The amorphous state of this phase was verified by HRTEM imaging and corresponding FFTs (b, c). In S2106, amorphous silicates occur as larger pocket-like domains (BFTEM: d, e). The rimmed nano-inclusions (arrow) in these pockets are also surrounded by amorphous silicate material (f).

TABLE 2. Composition of the amorphous silicate material within the GEMS-like phase of S2113 and the pocket-like domain of S2106 compared with GEMS-like material in Paris (atom%).

	Mg/Si	Fe/Si	S/Si	Al/Si	Ca/Si	Ni/Si
Pocket-like domain S2106	0.88	0.34	0.10	0.05	0.003	0.03
GEMS-like object S2113	0.86	0.57	0.16	0.10	0.005	0.07
GEMS-like object (Leroux et al., 2015)	0.71	0.68	0.29	0.06	0.012	0.05

similar Mg-content to the larger GEMS-like domain in S2113. No GEMS-like particles were found in lamella S2025.

Alteration Degree of Lamellae Based on TCI Compositions

TCIs and serpentine minerals in various shapes are common in Winchcombe, and both Mg-rich and Fe-rich examples occur. However, the phyllosilicate component of most of the TCI-like grains is enriched in Mg (Figure 9a and Figure S10). In Figure 9a, the TCI-like

phases and the Fe-rich phyllosilicates plot within the triangle defined by the compositions of TCI (a mixture of tochilinite and cronstedtite), and Fe-rich and Mg-rich serpentines, revealing similarities to previous analyses of CM chondrites (McSween Jr., 1987; Pignatelli et al., 2016). Rubin et al. (2007) and Lentfort et al. (2021) showed that the S/SiO_2 and "FeO"/SiO_2 ratios of TCIs can be used to define a more precise petrologic type of less altered CM2 lithologies. Rubin et al. (2007) determined threshold values for "FeO"/SiO_2 ratios that allow assignment to a petrologic subtype. They determined that an "FeO"/SiO_2 ratio of 1.5–1.7 is the limit for CM2.2/2.3, 2.0 for CM2.4/2.5, and 3.3 for CM2.6/2.7. Lentfort et al. introduced a value of 4.0 for CM2.8 and a value of 7.0 for CM2.9. In this study, the assignment of the petrologic subtype of TCI.a-c was used in accordance with these thresholds of Rubin et al., 2007 and Lentfort et al. (2021). Suttle et al. (2024) assigned a wide range of TCI compositions for the "clastic" matrix in Winchcombe. Their "FeO"/SiO_2 and S/SiO_2 values range from 1.28 to 4.04 and 0.01 to 0.86, respectively.

In Figure 9b, the "FeO"/SiO_2 and S/SiO_2 ratios of our TCI*-like phases and the lithologies A, B, C, E, H, and G of Winchcombe are compared to some CM chondrite fragments measured by Lentfort et al. (2021). The TCIs of Winchcombe show lower ratios of "FeO"/SiO_2 and S/SiO_2 than fragments of the other meteorites.
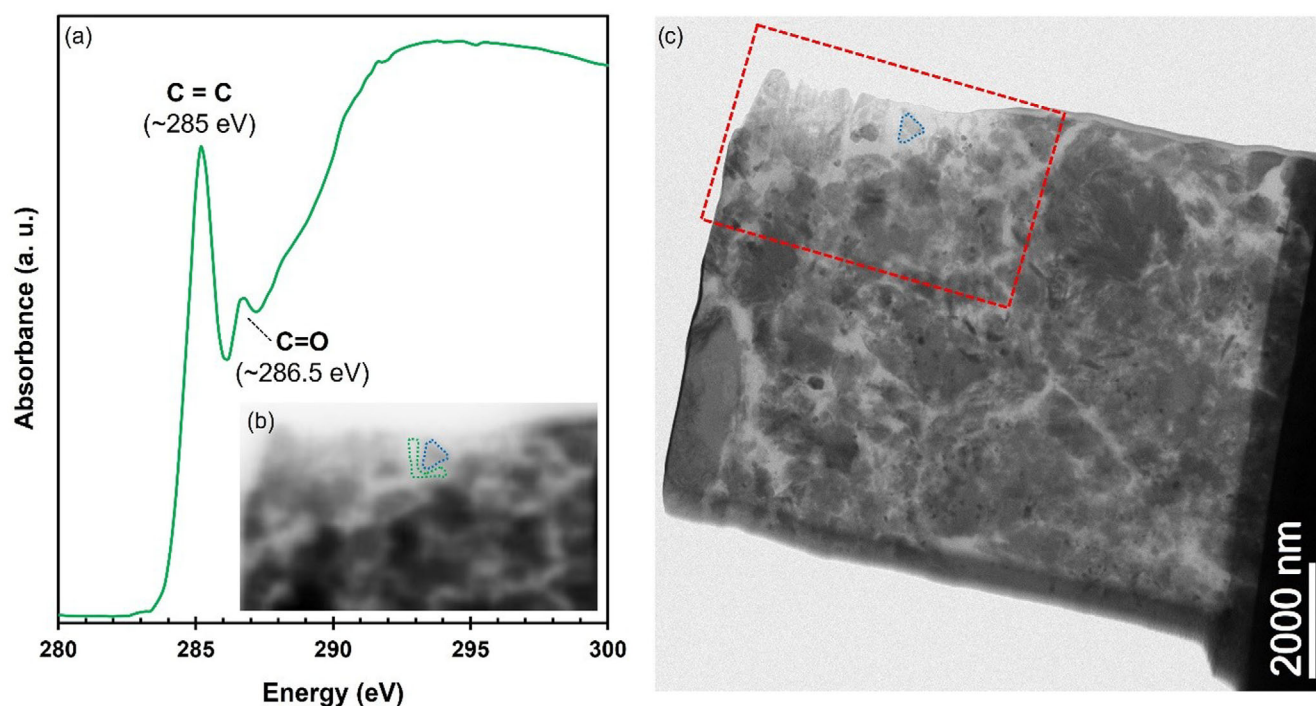
FIGURE 8. TEM and STXM images of the organic matter around the "GEMS-like" domain in S2113. (a) XANES spectrum of the region of interest, demonstrating the high abundance of aromatic units at ~285 eV and some C-O bonding at ~286.6 eV, typical of meteoritic organic matter, (b) STXM absorption image at 278 eV with the OM rim marked in green and the GEMS-like phase in blue, (c) BFTEM overview image of the lamella with the STXM map from (b) marked.
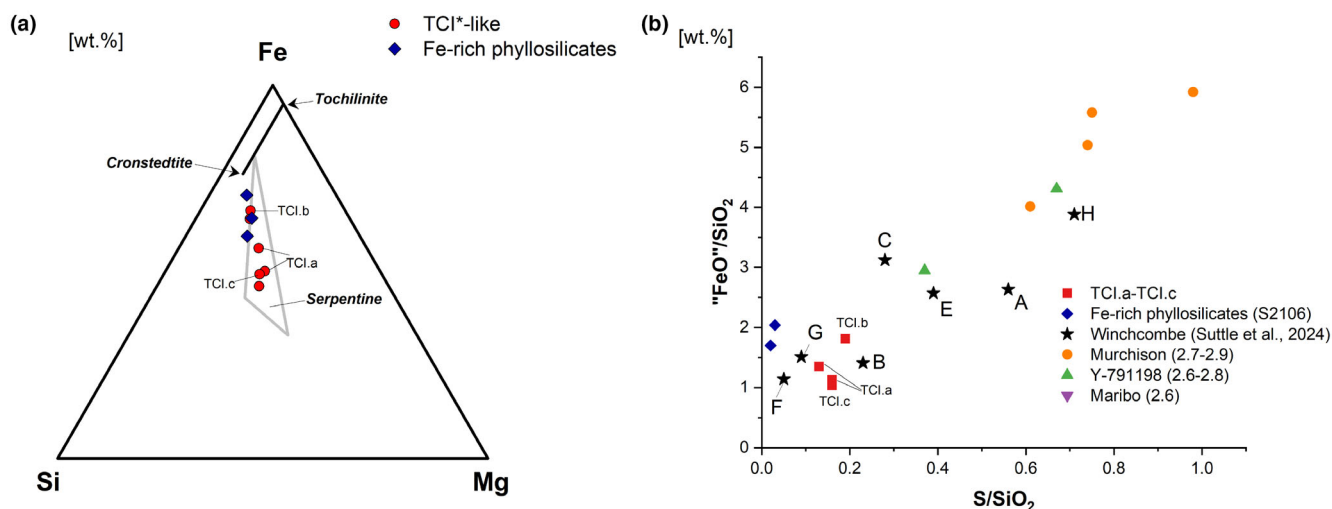

FIGURE 9. Composition of the TCI*-like phases corresponding to TCI.a-c, two TCI fragments of S2113 and S2025, and three Fe-rich phyllosilicates from S2106 and S2113 (Figures S3 and S5) in the lamellae. (a) In ternary Mg-Fe-Si space (wt%), the mineralogy of the TCI-like phases is dominated by solid solution of serpentine-like minerals. The triangle is defined by the compositions of TCI (a mixture of tochilinite and cronstedtite = black line), and Fe-rich and Mg-rich serpentines (McSween Jr., 1987; Pignatelli et al., 2016). (b) The S/SiO$_2$-"FeO"/SiO$_2$ plot shows that analyzed Winchcombe TCIs (TCI.a-TCI.c) show a higher alteration degree than other, more pristine fragments of CM2s like Maribo, Y-791198 and Murchison (Lentfort et al., 2021) and a similar alteration degree like lithologies B, F, and G of Winchcombe (Suttle et al., 2024). However, those data were acquired by electron microprobe analysis mooperating on larger length scales (see text for details).

This appears consistent with a higher alteration degree of our investigated Winchcombe lamellae compared with these more pristine CM chondrite fragments of Maribo, Y-791198, and Murchison (Lentfort et al., 2021). However, it should be kept in mind that TCI analyses in the Lentfort et al. work were acquired by electron microprobe, where the contribution of surrounding Fe-S-rich matrix material to analyses is more significant compared to STEM-EDX analyses in this work because of the larger excitation volume and that our TCI-like phases are a mixture of TCIs and serpentine minerals. However, it is still valuable to compare the two different approaches and to demonstrate the accuracy of the broader microprobe analyses in relation to the nanoscale TEM investigations. Still, according to this classification scheme, TCI.c would correlate with a lower subtype of ~2.0–2.1 of lamella S2113, although this is somewhat at odds with the finding of more pristine material such as the GEMS-like phase within the same lamella. TCI.a in S2025 would point to a similar petrologic subtype (~2.1), whereas TCI.b within lamella S2113 gives a higher petrologic subtype of ~2.3. This underlines the alteration complexity of the clastic matrix in Winchcombe on a submicron scale. TCI investigations in Winchcombe by Suttle et al. (2024) give, in most lithologies like A, B, C, and E, similar ratios and a generally higher alteration extent of ~2.1, so it is reasonable to assign measured TCIs to that petrologic subtype.

Figure 9b also shows the "FeO"-SiO_2 and S/SiO_2 values of some TCIs from Suttle et al. (2024), revealing similarities to the lithologies B, F, and G. In general, it can be concluded that all three TCIs in both lamellae from the clastic matrix show heterogeneous compositions consistent with a heterogeneously and strongly altered matrix (~CM2.0 to CM2.3).

DISCUSSION

The Winchcombe meteorite is a regolith breccia derived from a near-surface region of the CM parent body (Suttle et al., 2024). This implies a large heterogeneity, which is clearly reflected in our results by the sub-μm mineralogy and petrography of the three lamellae. Jenkins et al. (2023) concluded that some Winchcombe fragments show signs of terrestrial alteration because a variety of phases such as carbonates and Ca-sulfates may form over different time scales. Our results show that the studied Winchcombe lamellae have undergone little to no terrestrial alteration because no sulfates or ferrihydrites were documented. However, one larger carbonate grain in S2106 filling a crack could suggest a terrestrial origin (Figure 2f and Figure S1). Furthermore, the generally low temperature (<150°C) experienced by the Winchcombe matrix postulated by

King et al. (2022) can be confirmed, as no evidence of thermal metamorphism such as graphitized organic matter, which would show a completely different signature with sharp π* absorption at the carbon K-edge by STXM, or exsolved chromites was found at high resolution.

There is evidence that aqueous alteration did not progress in Winchcombe after breccia formation (Suttle et al., 2024). However, the extent of parent body alteration varies because it was significantly influenced by particular microenvironments and the compositions of the fluids (e.g., Bland et al., 2009; Pignatelli et al., 2016). The transport of elements played a dominant role for the different microenvironments at the scale of hundreds of micrometers in CM chondrites (e.g., Lindgren et al., 2017; Rubin et al., 2007; Suttle et al., 2021). Velbel et al. (2012) extended a conceptual model by Hanowski and Brearley (2001) with five stages of alteration in which the minerals at the earliest stages were dominated by Fe over Mg, leading to early-formed cronstedtite in the fine-grained and reactive matrix. Due to the continued reaction of the remaining coarser and/or more magnesian primary minerals, Mg gained a more dominant role over Fe in the aqueous solution. However, even though Winchcombe shows these varying degrees of aqueous alteration, some very pristine matrix areas, which give us insight into the initial mineralogy of the CM parent body, were detected in this work.

Occurrence of Amorphous Material

Lamella S2113 is exemplary for the petrographic heterogeneity of the clastic matrix, which is evident in the parallel occurrence of variable alteration phenomena and pristine phases. GEMS-like grains (Figures 6 and 7b,c), amorphous silicate material, and an alumina grain all occur within several μm in this lamella. Furthermore, radiating and fibrous TCI-like phases, Fe-Ni sulfides such as pentlandite, an isolated apatite with well-developed crystal faces, and a great variability of phyllosilicate textures are also observed. Each of these mineral phases likely formed through different stages of aqueous alteration on the CM parent body.

The occurrence of GEMS-like material in Winchcombe is of particular interest in this respect. Fe-rich and S-poor grains in GEMS-like material have also been found in the mildly altered Paris meteorite (Leroux et al., 2015), where the sizes of Fe-rich and S-free nanoparticles are comparable to those observed in our work. The slightly higher oxygen contents and lower mass number in the nanoparticle rims in our work are also similar to GEMS-like areas in Paris (Villalon et al., 2021) and could likely be alteration rims. Similar rims have only been observed in one more phase in S2113 and in some pocket-like domains in S2106, indicating a

different alteration regime in those areas, as these alteration rims were not found in the abundant sulfides surrounding these amorphous grains. The pyrrhotite/troilite aggregate at the rim of the GEMS-like phase is also unusual compared with other sulfides in the lamella, indicating a different formation regime here as well. It could have formed by condensation and subsequent sulfurization under reducing conditions based on the intact rim texture (Figure 6) (Lauretta et al., 1997; Schrader et al., 2021) or through a fluid with enhanced sulfur activity.

Studies by Ishii et al. (2018) and Schulz et al. (2024) on actual GEMS from cometary interplanetary dust particles (IDPs) show that the amorphous silicates of the IDPs are often coated by different types of organics. In addition, GEMS grains from IDPs show near-solar relative abundances of the rock-forming elements, a mean grain size of ~180 nm, and nanometer-sized inclusions of kamacite and iron-rich sulfide embedded in a magnesium-rich amorphous silicate (Ishii et al., 2018; Schulz et al., 2024; Villalon et al., 2021), making them very comparable to the GEMS-like phase in S2113 and the material in Paris. Aggregation in cold environments is suggested as a formation scenario for GEMS in IDPs, which strengthens the connection to presolar interstellar dust. In the case of the GEMS-like phase in S2113, it shows clear indications of formation and alteration in a different regime than the surrounding minerals. Furthermore, the organic matter encapsulating the GEMS-like phase could have played an important role by protecting it from extensive aqueous alteration, even though both the GEMS-like phase and organic matter show signs of minor hydration.

It has been suggested that the components of an original, hypothetical CM3 chondrite matrix included GEMS, GEMS-like domains, amorphous phases, Fe-Ni metals, Fe sulfides, and anhydrous silicates (Leroux et al., 2015; Suttle et al., 2021). In particular, amorphous silicates are an indicator of low alteration degree as they are metastable and prone to crystallization. Therefore, these materials presumably had a higher abundance prior to aqueous alteration in fine-grained materials (Chizmadia & Brearley, 2008). Lamella S2113 can therefore be regarded as a snapshot of this evolutionary trend as it contains not only pristine domains such as GEMS-like regions or refractory materials like the alumina grain, but also phyllosilicates and TCIs indicative of more advanced aqueous alteration.

Progress of the Aqueous Alteration tracked by TCI and Sulfide Mineralogy

TCIs are emblematic secondary aggregates in CM chondrites that likely formed from Fe-Ni metals, anhydrous silicates, and carbonates. They record highly complex developing fluid compositions but generally illustrate early transformation activity on the parent body (Pignatelli et al., 2016). However, serpentine-type minerals are also found throughout all lamellae, which point to more advanced alteration, as they accumulate Mg with proceeding alteration degree (e.g., Zega et al., 2006; Zolensky et al., 1993). Vein textures and d-values of 0.73 nm, consistent with chrysotile, indicate these areas of more extensive alteration (Downs & Hall-Wallace, 2003; Suttle et al., 2021; Zolensky et al., 1993). In particular, at the upper right margin of lamella S2113, vein-like textures and a gradual degree of crystallization of the phyllosilicates indicate a variable but extensive degree of alteration, as phyllosilicate morphologies vary between fine-grained to coarser, fibrous, and elongated. Lamella S2113 has therefore recorded a petrographic snapshot of initial and advanced alteration on a sub-μm scale.

Lamella S2025 shows different petrography compared with S2113, indicative of a different microenvironment active in this part of Winchcombe before lithification into the final rocks or in a pre-accretionary setting. GEMS-like domains or amorphous silicates were not detected in S2025, but one large distinct TCI-like phase dominates about one third of the lamella. This dominant large TCI-like component exhibits a typical fibrous texture with nanocrystalline tochilinite fibers intergrown with cronstedtite and serpentine (Figure 4c). Most of the analyzed TCI-like grains of the matrix are intermixed with serpentine minerals (Figure 9 and Figure S10) showing comparable results to previous analyses of CM chondrite matrices (McSween Jr., 1987). Other serpentine-type minerals in this lamella show textural similarities with those of the other lamellae, with either blocky and/or fibrous morphologies. A high density of Fe-Ni sulfides is observed in S2025. A few ~300 nm-sized sulfides also show euhedral crystal faces (Figure 5a). Pentlandite in particular was identified at high resolution by its typical Ni-rich chemistry and distinct d-values (Figure 5c,f). The occurrence of this mineral in CM2 chondrites is considered to be a product of advancing parent body alteration of previously formed sulfides, tochilinite, and metals (Harries & Langenhorst, 2013), with increasing abundance seemingly correlating with the degree of aqueous alteration relative to other chondritic materials (Chokai et al., 2004). According to the Rubin scale, a petrologic subtype of 2.2 is associated with the frequent occurrence of pentlandite (Rubin et al., 2007). Formation of Fe-Ni sulfides could be related to alteration of primary pyrrhotite. Singerling and Brearley (2020) demonstrated that primary pyrrhotite is unstable in CM and CR chondrites and transformed into alteration products such as secondary pentlandite,

magnetite, and phyllosilicates. One pentlandite grain shows a serpentine fiber indicating subtle further alteration (Figure 5c), but distinct alteration phenomena such as polyhedral serpentine minerals, vein-like textures, or alteration fronts such as observed in the other lamella could not be recognized here. Lamella S2025 therefore seems to show a generally higher degree of alteration than lamella S2113 because of the more frequent occurrence of pentlandite and the absence of amorphous domains. Mg-rich polyhedral serpentine minerals are furthermore indicative of more intense aqueous alteration, as discussed above. However, TCI mineralogy indicates a lower degree of alteration, which underlines the alteration complexity of the Winchcombe meteorite on the sub-µm scale.

Finally, lamella S2106 was extracted from lithology H, which was tentatively assigned as 2.3/2.4 by Suttle et al. (2024). However, this is the least abundant lithology in Winchcombe, at 0.2%, while the matrix occurs at 15.4% (Suttle et al., 2024). S2106 is characterized on the submicron scale by containing no coarser TCI grains but generally larger and well-crystallized Fe-rich phyllosilicates.

The lack of TCI-like phases makes it impossible to assign a petrologic type here based on TCI mineralogy. However, the generally high Fe content of phyllosilicates seems to indicate a less advanced alteration stage when compared to the lamellae with Mg-rich serpentines discussed above. It could also be related to the selective alteration of reactive Fe-host minerals, which corresponds to stage 2 of the conceptual model of Velbel et al. (2012). S2106 also has a higher porosity than the lamellae from the matrix; it does not only contain a small amount of pentlandite, but also a comparable amount of FeS sulfides with no Ni, and it also contains some amorphous domains. These observations are in line with a less advanced alteration stage and support the initial assessment of lithology H by Suttle et al. (2024). However, it also shows that a distinct petrologic subtype for a very rare subunit is difficult to define (Suttle et al., 2024).

We conclude that the general phyllosilicate and TCI mineralogy of the three lamellae investigated in this study agree with the alteration states inferred in previous work on a larger scale by, for example, Suttle et al. (2024) and Daly et al. (2024). However, we also observe sub-µm heterogeneities such as heavily altered Mg-rich phyllosilicates next to pristine GEMS-like and amorphous regions. This heterogeneity emphasizes the extreme complexity of CM chondrite breccias and of carbonaceous meteorites in general, as well as the importance of detecting new, terrestrially unaltered and freshly observed meteorite falls to unravel the complex alteration history. Analyses of such observed meteorite falls allow us to differentiate between alteration effects on the CM parent body and on Earth and to test whether proxies on meteorite finds compared to less altered falls are still applicable.

CONCLUSIONS

Winchcombe is an observed CM2 chondrite fall that shows a wide range of mineralogical and petrographic characteristics with minimal terrestrial alteration, which enables the disentangling of the complex evolution of primary and secondary phases on a volatile-rich parent body. In this work, three lamellae from the clastic matrix and lithology H (as defined by Suttle et al., 2024) in the Winchcombe meteorite were investigated by TEM techniques to infer the mineralogy, petrography, and alteration history. The following main conclusions can be drawn:

1. TCI-like morphologies are mainly type II and range from irregular to radial. The chemistry of the TCI-like grains gives a petrologic subtype of ~2.0–2.3, which is generally consistent with other work on a larger scale using SEM.
2. The crystallography of phyllosilicates investigated by HRTEM is dominated by serpentine-type minerals, specifically the chrysotile polymorph. Clay-type minerals such as those found in highly altered CI chondrites, Ryugu, or Bennu have not been found; this confirms the different alteration regime on the CM parent body compared to CI-like materials. The Mg-rich chemistry of the phyllosilicates points to a generally high degree of alteration of the Winchcombe matrix when compared to other CM chondrites such as Murchison or Maribo.
3. The sulfides in each lamella are mainly pentlandite, which supports the generally higher degree of alteration. Minerals indicative of terrestrial alteration, such as sulfates or ferrihydrite, have not been found, supporting the generally low degree of terrestrial alteration.
4. However, despite the generally low petrologic subtype of the three lamellae, a few pristine materials such as amorphous silicates, GEMS-like phases, and organic matter were detected. Therefore, alteration extents may differ from lamella to lamella at the micro- to nanoscale. It is, therefore, possible to track the entire evolution of water–rock reactions on the CM parent body at the sub-µm scale.
5. The spatially associated highly altered and unaltered materials can be explained by heterogeneous chemical microenvironments on the CM parent body as well as intense brecciation and mixing processes.

Data Availability Statement—The TEM/STEM/EDX processed data generated in this study have been deposited in the research data repository NextCloud of the Universität Münster. Additional images and processed TEM data generated in this study are provided in the Supporting Information. The data that support the findings of this study are available from the corresponding author upon reasonable request.

Editorial Handling—Dr. Yves Marrocchi

REFERENCES

Barber, D. J. 1981. Phyllosilicates and Other Layer-Structured Minerals in Stony Meteorites. *Clay Minerals* 20: 415–454.

Bland, P. A., Jackson, M. D., Coker, R. F., Cohen, B. A., Webber, J., Beau, E., Lee, M. R., et al. 2009. Why Aqueous Alteration in Asteroids Was Isochemical: High Porosity ≠ High Permeability. *Earth and Planetary Science Letters* 287: 559–568.

Brearley, A. J. 2006. The Action of Water. *Meteorites and the Early Solar System II* 943: 587–624.

Chizmadia, L. J., and Brearley, A. J. 2008. Mineralogy, Aqueous Alteration, and Primitive Textural Characteristics of Fine-Grained Rims in the Y-791198 CM2 Carbonaceous Chondrite: TEM Observations and Comparison to ALHA81002. *Geochimica et Cosmochimica Acta* 72: 602–625.

Chokai, J., Zolensky, M., Le, L., Nakamura, K., Mikouchi, T., Monkawa, A., Koizumi, E., and Miyamoto, M. 2004. Aqueous Alteration Mineralogy in CM Carbonaceous Chondrites (abstract #1506). *35th Lunar and Planetary Science Conference*.

Ciesla, F. J., Lauretta, D. S., Cohen, B. A., and Hood, L. L. 2003. A Nebular Origin for Chondritic Fine-Grained Phyllosilicates. *Science* 299: 549–552.

Daly, L., Suttle, M. D., Lee, M. R., Bridges, J., Hicks, L., et al. 2024. Brecciation at the Grain Scale within the Lithologies of the Winchcombe Mighei-Like Carbonaceous Chondrite. *Meteoritics & Planetary Science* 59: 1068–1100.

Downs, R. T., and Hall-Wallace, M. 2003. The American Mineralogist Crystal Structure Database. *American Mineralogist* 88: 247–250.

Fuchs, L. H., Olsen, E., and Jensen, K. J. 1973. Mineralogy, Mineral-Chemistry, and Composition of the Murchison (C2) Meteorite. *Smithsonian Contributions to the Earth Sciences* 10: 1–39.

Hanowski, N. P., and Brearley, A. J. 2001. Aqueous Alteration of Chondrules in the CM Carbonaceous Chondrite, Allan Hills 81002: Implications for Parent Body Alteration. *Geochimica et Cosmochimica Acta* 65: 495–518.

Harries, D., and Langenhorst, F. 2013. The Nanoscale Mineralogy of Fe,Ni Sulfides in Pristine and Metamorphosed CM and CM/CI-Like Chondrites: Tapping a Petrogenetic Record. *Meteoritics & Planetary Science* 48: 879–903.

Hewins, R. H., Bourot-Denise, M., Zanda, B., Leroux, H., Barrat, J. A., Humayun, M., Göpel, C., et al. 2014. The Paris Meteorite, the least Altered CM Chondrite So Far. *Geochimica et Cosmochimica Acta* 124: 190–222.

Ishii, H. A., Bradley, J. P., Bechtel, H. A., Brownlee, D. E., Bustillo, K. C., Ciston, J., Cuzzi, J. N., Floss, C., and Joswiak, D. J. 2018. Multiple Generations of Grain Aggregation in Different Environments Preceded Solar System Body Formation. *Proceedings of the National Academy of Sciences of the United States of America* 115: 6608–13.

Jenkins, L. E., Lee, M. R., Daly, L., King, A. J., Floyd, C. J., Martin, P.-E., Almeida, N. V., and Genge, M. J. 2023. Winchcombe: An Example of Rapid Terrestrial Alteration of a CM Chondrite. *Meteoritics & Planetary Science* 59: 988–1005.

Kimura, M., Imae, N., Komatsu, M., Barrat, J. A., Greenwood, R. C., Yamaguchi, A., and Noguchi, T. 2020. The most Primitive CM Chondrites, Asuka 12085, 12169, and 12236, of Subtypes 3.0–2.8: Their Characteristic Features and Classification. *Polar Science* 26: 1–15.

King, A. J., Daly, L., Rowe, J., Joy, K. H., Greenwood, R. C., Devillepoix, H. A. R., Suttle, M. D., et al. 2022. The Winchcombe Meteorite, a Unique and Pristine Witness from the Outer Solar System. *Science Advances* 8: 1–17.

Lauretta, D. S., Lodders, K., and Fegley, B. 1997. Experimental Simulations of Sulfide Formation in the Solar Nebula. *Science* 277: 358–360.

Lee, M. R., Lindgren, P., Sofe, M. R., O'D Alexander, C. M., and Wang, J. 2012. Extended Chronologies of Aqueous Alteration in the CM2 Carbonaceous Chondrites: Evidence from Carbonates in Queen Alexandra Range 93005. *Geochimica et Cosmochimica Acta* 92: 148–169.

Lee, M. R., Sofe, M. R., Lindgren, P., Starkey, N. A., and Franchi, I. A. 2013. The Oxygen Isotope Evolution of Parent Body Aqueous Solutions as Recorded by Multiple Carbonate Generations in the Lonewolf Nunataks 94101 CM2 Carbonaceous Chondrite. *Geochimica et Cosmochimica Acta* 121: 452–466.

Lentfort, S., Bischoff, A., Ebert, S., and Patzek, M. 2021. Classification of CM Chondrite Breccias—Implications for the Evaluation of Samples from the OSIRIS-REx and Hayabusa 2 Missions. *Meteoritics & Planetary Science* 56: 127–147.

Leroux, H., Cuvillier, P., Zanda, B., and Hewins, R. H. 2015. GEMS-Like Material in the Matrix of the Paris Meteorite and the Early Stages of Alteration of CM Chondrites. *Geochimica et Cosmochimica Acta* 170: 247–265.

Lindgren, P., Lee, M. R., Starkey, N. A., and Franchi, I. A. 2017. Fluid Evolution in CM Carbonaceous Chondrites Tracked through the Oxygen Isotopic Compositions of Carbonates. *Geochimica et Cosmochimica Acta* 204: 240–251.

Mackinnon, I. D. R., and Zolensky, M. E. 1984. Proposed Structures of Poorly Characterized Phases in C2M Carbonaceous Chondrite Meteorites. *Nature* 309: 240–42.

Marrocchi, Y., Rigaudier, T., Piralla, M., and Piani, L. 2023. Hydrogen Isotopic Evidence for Nebular Pre-Hydration and the Limited Role of Parent-Body Processes in CM Chondrites. *Earth and Planetary Science Letters* 611: 118151.

McSween, H. Y., Jr. 1987. Aqueous Alteration in Carbonaceous Chondrites: Mass Balance Constraints on Matrix Mineralogy. *Geochimica et Cosmochimica Acta* 51: 2469–77.

Metzler, K., Bischoff, A., and Stöffler, D. 1992. Accretionary Dust Mantles in CM Chondrites: Evidence for Solar Nebula Processes. *Geochimica et Cosmochimica Acta* 56: 2873–97.

Nakamura, T., and Nakamuta, Y. 1996. X-Ray Study of PCP from the Murchison CM Carbonaceous Chondrite. *Proceedings of the NIPR Symposium on Antarctic Meteorites* 9: 37–50.

Pignatelli, I., Marrocchi, Y., Mugnaioli, E., Bourdelle, F., and Gounelle, M. 2017. Mineralogical, Crystallographic and Redox Features of the Earliest Stages of Fluid Alteration in CM Chondrites. *Geochimica et Cosmochimica Acta* 209: 106–122.

Pignatelli, I., Marrocchi, Y., Vacher, L. G., Delon, R., and Gounelle, M. 2016. Multiple Precursors of Secondary Mineralogical Assemblages in CM Chondrites. *Meteoritics & Planetary Science* 51: 785–805.

Rubin, A. E. 2015. An American on Paris: Extent of Aqueous Alteration of a CM Chondrite and the Petrography of its Refractory and Amoeboid Olivine Inclusions. *Meteoritics & Planetary Science* 50: 1595–1612.

Rubin, A. E., Trigo-Rodríguez, J. M., Huber, H., and Wasson, J. T. 2007. Progressive Aqueous Alteration of CM Carbonaceous Chondrites. *Geochimica et Cosmochimica Acta* 71: 2361–82.

Schrader, D. L., Davidson, J., McCoy, T. J., Zega, T. J., Russell, S. S., Domanik, K. J., and King, A. J. 2021. The Fe/S Ratio of Pyrrhotite Group Sulfides in Chondrites: An Indicator of Oxidation and Implications for Return Samples from Asteroids Ryugu and Bennu. *Geochimica et Cosmochimica Acta* 303: 66–91.

Schulz, B., Vollmer, C., Leitner, J., Keller, L. P., and Ramasse, Q. M. 2024. Petrographic and Chemical Characterization and Carbon and Nitrogen Isotopic Compositions of Cometary IDPs and their GEMS Amorphous Silicates. *Geochimica et Cosmochimica Acta* 378: 153–167.

Singerling, S. A., and Brearley, A. J. 2020. Altered Primary Iron Sulfides in CM2 and CR2 Carbonaceous Chondrites: Insights into Parent Body Processes. *Meteoritics & Planetary Science* 55: 496–523.

Suttle, M. D., Daly, L., Jones, R. H., Jenkins, L., Van Ginneken, M., Mitchell, J. T., Bridges, J. C., et al. 2024. The Winchcombe Meteorite—A Regolith Breccia from a Rubble Pile CM Chondrite Asteroid. *Meteoritics & Planetary Science* 59: 1043–67.

Suttle, M. D., King, A. J., Schofield, P. F., Bates, H., and Russell, S. S. 2021. The Aqueous Alteration of CM Chondrites, a Review. *Geochimica et Cosmochimica Acta* 299: 219–256.

Tomeoka, K., and Buseck, P. R. 1985. Indicators of Aqueous Alteration in CM Carbonaceous Chondrites: Microtextures of a Layered Mineral Containing Fe, S, O and Ni. *Geochimica et Cosmochimica Acta* 49: 2149–63.

Vacher, L. G., Truche, L., Faure, F., Tissandier, L., Mosser-Ruck, R., and Marrocchi, Y. 2019. Deciphering the Conditions of Tochilinite and Cronstedtite Formation in CM Chondrites from Low Temperature Hydrothermal Experiments. *Meteoritics & Planetary Science* 54: 1870–89.

Velbel, M. A. 2014. Stoichiometric Reactions Describing Serpentinization of Anhydrous Primary Silicates: A Critical Appraisal, with Application to Aqueous Alteration of Chondrule Silicates in CM Carbonaceous Chondrites. *Clays and Clay Minerals* 62: 126–136.

Velbel, M. A., Tonui, E. K., and Zolensky, M. E. 2012. Replacement of Olivine by Serpentine in the Carbonaceous Chondrite Nogoya (CM2). *Geochimica et Cosmochimica Acta* 87: 117–135.

Villalon, K. L., Ohtaki, K. K., Bradley, J. P., Ishii, H. A., Davis, A. M., and Stephan, T. 2021. Search for Meteoritic GEMS II: Comparison of Inclusions in Amorphous Silicates from the Paris Chondrite and from Anhydrous Chondritic Interplanetary Dust Particles. *Geochimica et Cosmochimica Acta* 310: 346–362.

Vollmer, C., Leitner, J., Kepaptsoglou, D., Ramasse, Q. M., Mosberg, A. B., King, A. J., Bays, C. L., Schofield, P. F., and Araki, T. 2024. High-Spatial Resolution Functional Chemistry of Nitrogen Compounds in the Observed UK Meteorite Fall Winchcombe. *Nature Communications* 15: 778–788.

Wise, D. U., Dunn, D. E., Engelder, J. T., Geiser, P. A., Hatcher, R. D., Kish, S. A., Odom, A. L., and Schamel, S. 1984. Fault-Related Rocks: Suggestions for Terminology. *Geology* 12: 391–94.

Zega, T. J., Garvie, L. A. J., Dódony, I., Friedrich, H., Stroud, R. M., and Buseck, P. R. 2006. Polyhedral Serpentine Grains in CM Chondrites. *Meteoritics & Planetary Science* 41: 681–88.

Zolensky, M., Barrett, R., and Browning, L. 1993. Mineralogy and Composition of Matrix and Chondrule Rims in Carbonaceous Chondrites. *Geochimica et Cosmochimica Acta* 57: 3123–48.

SUPPORTING INFORMATION

Additional supporting information may be found in the online version of this article.

Figure S1. TEM micrographs and EDX maps of TCI-like grains and accessory phases. (a) Apatite in S2113 with well-developed crystal faces. Next to the radial fan-shaped TCI.b in S2113, an AlO-rich grain was detected by STEM-EDX. The grain shows strong diffraction contrast but no d-spacing could be determined (c). TCI.c in S2113 encloses a Ni-P rich grain (d). An elongated phase in contact with organic matter shows vein-like structures and fibers in S2113 (arrows) (e). HAADF image and EDX map of a calcite grain in S2106 (rectangle in Fig. 2e).

Figure S2. TEM micrographs and HRTEM images of variable phyllosilicate and TCI textures in Winchcombe. (a, b) Fibrous phyllosilicates in S2025. (c, d) Fibrous phyllosilicates in S2106. (e, f) the blocky TCI fragment (Fig. 4e) in lamella S2113.

Figure S3. Fe-rich phyllosilicates in Winchcombe: (a) In S2106, blocky phyllosilicates occur (contour lines) indicate where two EDX analyses for Fig. 8 were performed). (b) In S2025, a blocky TCI-like fragment (encircled) is similar to the blocky phyllosilicates in TCI.a, and carbonates are also present in this region.

Figure S4. STEM-EDX maps (Fe-Ni, O, Si, Mg; a-d) of the GEMS-like domain in Winchcombe lamella S2113.

Figure S5. TEM micrographs of the alteration front within one of the Fe-rich phyllosilicates in S2113 (Fig.3d). The alteration front can be seen in BFTEM mode (a) as well as in EDX Fe-Mg composite maps by a slightly higher Mg content in the lower half of the grain (b). HRTEM imaging gives two different d values indicative of the serpentine polymorph lizardite.

Figure S6. STEM-EDX element maps of lamellae S2113 (a, b and c), S2025 (d, e and f) and S2106 (g and h).

Figure S7. TEM micrographs and EDX maps of lamella S2106 from lithology H. The lamella contains a GEMS-like ("pocket"-like domain; EDX analysis of region b was performed) region (a, b) with some inclusions), but is otherwise dominated by blocky and large phyllosilicates (STEM-HAADF: c–e).

Figure S8. TEM micrographs and EDX maps of the three TCIs (TCI.a in a, b and c; TCI.b in d, e and f; TCI.c in g, h and i) of lamellae S2025 and S2113. Note that the arrows are indicating S enriched fibers and that the encircled domains in f and i were analyzed for their chemical composition (Tables 1 and S1).

Figure S9. HAADF images and elemental maps of the Al and O enriched area. The arrows mark the AlO-rich grain which is also seen in Figure S1.

Figure S10. The ternary diagram with the elements Fe, Mg, Si shows the composition (in at.%) and components of the phyllosilicates that make up the coarser phyllosilicates and the TCI*-like phases in the lamellae of the Winchcombe matrix and Lithology H.

Table S1. Composition of TCI.a* including the Fe-rich phyllosilicates.